Perfect magnetic mirror and simple perfect absorber in the visible spectrum

C. A. Valagiannopoulos
Department of Radio Science and Engineering, School of Electrical Engineering, Aalto University, P.O. Box 13000, FI-00076 Aalto, Finland and Department of Electrical and Computer Engineering, University of Texas at Austin, 1616 Guadalupe Sreet, Texas 78712, USA

A. Tukiainen, T. Aho, T. Niemi, and M. Guina
Optoelectronics Research Centre, Tampere University of Technology, P.O. Box 527, FI-33101 Tampere, Finland

S. A. Tretyakov and C. R. Simovski
Department of Radio Science and Engineering, School of Electrical Engineering, Aalto University, P.O. Box 13000, FI-00076 Aalto, Finland
(Received 6 November 2014; revised manuscript received 17 February 2015; published 11 March 2015)

Known experimental artificial magnetic conductors for terahertz and optical frequencies are formed by arrays of nanoparticles of various shapes. In this paper, we show that artificial magnetic conductors for the visible spectrum can be realized as simple, effectively quasistatic resonating structures, where the effective inductance is due to the magnetic flux inside a uniform metal substrate, and the effective capacitance is due to electric polarization of a thin uniform dielectric cover. To illustrate the main potential application of artificial magnetic conductors, we concentrate on the perfect-absorption regime, achieved by adjusting the loss factor of the artificial magnetic conductor to match its real input impedance to free space. We provide approximate analytical design formulas and introduce a simple equivalent circuit to explain the physical mechanism of emulation of magnetic response and perfect absorption of light. A prototype of a nearly perfect absorber for optical (from green to ultraviolet) frequencies is designed and experimentally tested. The results confirm the theoretical predictions and show polarization insensitivity and angular independence of response in a wide range of incidence angles.

DOI: 10.1103/PhysRevB.91.115305 PACS number(s): 42.25.Bs, 13.40.−f, 42.82.Fv

I. INTRODUCTION

Ideal electric conductors reflect light reversing the phase of the electric field: the total tangential electric field on a perfectly conducting surface is zero. Although the conductivity of any material is finite, realization of nearly perfect mirror reflection does not present any significant challenge. In the microwave frequency range all common metals behave as nearly ideal electric conductors. On the other hand, magnetic conductors do not exist, because there are no free magnetic charges which could flow in a "magnetic conductor." Thus, realization of surfaces which behave as magnetic conductors, where the tangential *magnetic* field is zero on the mirror surface, is possible only within the paradigm of metamaterials and metasurfaces: artificial, structural materials [1,2] and surfaces [3–5] with electromagnetic properties not found in any natural material. In addition to the fundamental interest in emulating nonexisting magnetic currents, the ability to reflect light in phase is a very attractive feature, which can enable a number of applications in various frequency ranges. Antenna applications of artificial magnetic conductors are well developed, e.g., [6,7].

In the microwave frequency range, artificial magnetic conductors can be realized using resonant structures. The most common approach is to use an array of small metal patches separated from a metal surface by a thin dielectric layer (high-impedance surface) [3,8]. Here, the volume between the array and the conducting plane stores some magnetic energy, forming an inductor. In the gaps between the metal patches some electric field energy is stored, forming an effective capacitor. At the resonant frequency of this parallel resonant circuit the impedance experienced by the incident wave becomes very high, which emulates the boundary condition at a surface of a perfect *magnetic* conductor: the total tangential magnetic field on the surface is close to zero.

Unfortunately, this paradigm cannot be scaled to the visible frequencies, because at these frequencies metals are not behaving as good enough conductors. Only some limited theoretical and experimental results have been reported which utilize arrayed nanostructures, very sensitive in size and difficult to fabricate, such as fish-scale-shaped aluminum nanowires [9], carbon nanotubes [10], or cubic dielectric nanoresonators [11]. In this paper, we study the possibility of realizing an artificial magnetic conductor in the visible frequency range using the kinetic inductance of electrons inside metals as an inductor in a parallel-resonant circuit. We show that the regime of an absorbing magnetic wall can be realized in a simple thin layer of a dielectric (semiconductor) material on a metal surface. Indeed, polarized dielectrics can store electric field energy, and, by properly choosing the permittivity and thickness of a dielectric sheet, one can engineer the resonant frequency of the artificial magnetic conductor.

The most common application of artificial magnetic conductors is in the design of perfect absorbers for electromagnetic radiation. Indeed, at the frequency where the surface behaves as a perfect magnetic conductor, the reactive part of the surface impedance is infinite (and the corresponding reactive admittance is zero). Thus, it is enough to add a purely resistive sheet with the surface resistance equal to the free-space impedance (or appropriately choose the loss factor of the dielectric layer) in order to absorb all incident power without reflections. In the microwave frequency range this scenario can be realized as an artificial magnetic conductor formed by an array of metal patches over a ground plane, where the appropriate losses are due either to a resistive sheet on top of the structure [12] or to losses in the dielectric substrate [8]. In these microwave realizations, the effective inductor which stores reactive magnetic field energy is due to the spacing

between the highly conducting ground planes (an external inductance due to fields outside of conductors). In contrast, in the structure studied in this paper the reactive magnetic energy is stored inside the metallic substrate (internal, kinetic inductance due to magnetic flux inside the metal).

The resonant response of optically thin layers, potentially leading to magnetic-wall response and nearly perfect absorption, can be realized in carefully designed arrangements of subwavelength unit cells of various shapes and materials, for example, using nanobar arrays near a gold film [13], cut-wire arrays [14], nanosphere arrays [15], and other nanostructured layers, e.g., [16–18]. The common element of the aforementioned works is again (as in the problem of constructing optical magnetic walls) the usage of nanocomponents (bars, trapezoidal rods, cylinders, rings) to formulate a surface which can act as a good absorber of light. On the other hand, relatively few studies have been published on the absorption in the visible with the sole use of bulk materials. For example, strong frequency dispersion in reflection, typical for resonant structures, was noticed in [19], but the structure has not been optimized and accordingly the reflectivities are not optimal.

In this paper, we demonstrate, both theoretically and experimentally, a nearly perfectly absorbing artificial magnetic conductor in the visible frequency range. The proposed structure is extremely simple: it consists of a layer of metal (needed to store magnetic energy and provide the necessary effective inductance) covered by a thin dielectric layer (needed to store electric energy and provide the necessary effective capacitance). We present a systematic approach to model and design optimal resonant layers and absorbers for optical frequencies with the use of very thin layers deposited above metallic substrates. From the numerous combinations of materials and sizes giving a quasiperfect absorber, we picked one which is easily realizable, and fabricated a corresponding prototype comprised of a gold substrate, a thin germanium layer above it (only 6 nm) and a thicker silicon nitride superstrate (less than 30 nm). As shown both analytically and experimentally, the proposed design exhibits high efficiency (less than 8% of the power reflects back) within a very wide frequency range of absorption (covering the ultraviolet, violet, blue, and partially the green spectrum) and simultaneously it is very thin from both the physical and optical points of view. Furthermore, it is functional even for quite oblique incident rays (up to 60° from the normal axis), works well for both polarizations, and, above all, is extremely simple as a structure. Based on this unique combination of beneficial characteristics, we are confident that this specific optimal configuration can be used in a wide range of applications from photonics (photosensitive surfaces) and signal processing (optical filters and switches) to energy (photovoltaic devices) and commerce (optical tagging).

We note that the studied structure is similar to the structure recently investigated experimentally in [20]. Here, in contrast to that work, we provide a thorough physical justification and a complete description of the mechanism through which nearly perfect absorption is possible, and complement the analysis with an experimental validation of an optimized absorber. We prove that it is possible to compensate admittances in a thin layer in a quasistatic way, and not through a wave interference as described in [20]. Finally, we analyze the material-parameter limitations for the frequency ranges where an optically thin lossy magnetic wall can be realized with common metals as substrates and compare this absorption mechanism with that of the conventional Dallenbach absorber [21].

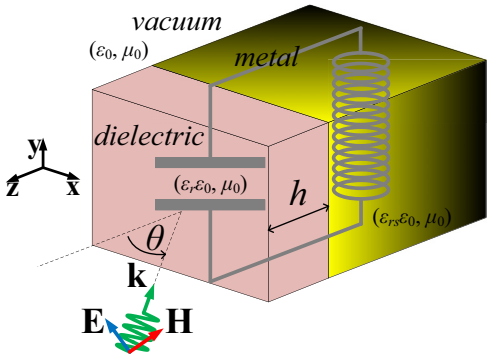

FIG. 1. (Color online) An artificial magnetic mirror formed by a thin dielectric layer with the relative permittivity $\mathrm{Re}(\varepsilon_r) > 1$ and thickness h on a bulk metal substrate [the relative permittivity $\mathrm{Re}(\varepsilon_{rs}) < 0$] excited by a plane wave $(\mathbf{E},\mathbf{H},\mathbf{k})$ traveling along a direction that forms an angle θ with the normal axis. The equivalent lossless resonant circuit is also depicted, illustrating the reactive components in the corresponding materials: capacitor for the layer, inductor for the substrate.

II. METHODS

A. General model of resonant magnetic walls

It is well known that if we consider an arbitrary structure developed along an axis, the condition to behave as a perfect magnetic conductor is vanishing input admittance: $Y_{\mathrm{in}} = 0$. Therefore, such a structure is lossless and the reactive parts of the components admittances are getting *neutralized* by each other (resonance). If we confine ourselves to the optical frequencies, the role of the inductor can be played by a (supposedly lossless) metallic bulk with purely negative permittivity $\varepsilon_r < 0$, while a thin layer (thickness h) of a common dielectric (for this discussion assumed to be lossless) with the relative permittivity $\varepsilon_r > 1$ can provide the capacitive load as shown in Fig. 1. Obviously, lossless metals do not exist, but we can ignore the resistive parts for the sake of simplicity in explaining this paradigm. An electromagnetic circuit appears excited by an obliquely incident plane wave of arbitrary polarization (TE or TM) advancing along a direction that forms an angle θ with the normal axis. Time dependence of the form $e^{-i2\pi ft}$ is considered and suppressed throughout the analysis, where $f = \frac{ck_0}{2\pi}$ is the operating frequency, $k_0 = \frac{2\pi}{\lambda_0}$ is the free-space wave number, and c is the speed of light. By λ_0, we denote the operating free-space wavelength. If we consider normal incidence $\theta = 0$ (where the two polarizations TE and TM are identical) and assume an optically thin slab ($k_0 h \ll 1$), the condition for perfect magnetic-wall reflection is written as the resonance in the formulated equivalent circuit between the inductor representing the currents flowing into the negative-permittivity metal and the capacitors emulating the behavior of a thin penetrable dielectric layer [22]:

$$Y_{\mathrm{in}} = \frac{1}{\eta_0}[\sqrt{\varepsilon_{rs}} - i(\varepsilon_r - 1)k_0 h] = 0. \quad (1)$$

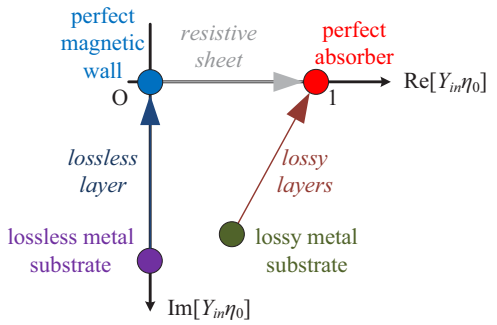

FIG. 2. (Color online) Schematic of the normalized complex input admittance plane $Y_{\rm in}\eta_0$ showing two alternative ways of realizing a perfect absorber for normal incidence. One can start from a lossless metallic substrate (purple dot) and with a lossless dielectric layer to obtain (via the deep blue arrow) a perfect magnetic-wall regime (the blue dot); to this end, the addition of a matched resistive sheet can lead (via the gray arrow) to a perfect-absorber regime (the red dot). More realistically, one can start from a lossy metallic bulk (the green dot) and by adding a suitably selected lossy layer (or layers) can reach again (via the brown arrow) the perfectly absorbing regime (the red dot).

The notation $\eta_0 = \sqrt{\frac{\mu_0}{\varepsilon_0}}$ is used for the wave impedance of free space (the background material in our configuration).

The aforementioned resonance is illustrated by Fig. 2. Beginning with a bulk metal of negative permittivity $\varepsilon_{\rm rs} < 0$ (the purple dot), one can add a suitable lossless dielectric layer of $\varepsilon_{\rm r} > 1$ (the blue arrow) to obtain a perfect magnetic wall (the blue dot). An effective magnetic response is created because induced currents in the metal substrate and in the dielectric layer are out of phase (as illustrated by the equivalent circuit), and they form an effective current loop. As mentioned above, the insertion of a matched purely resistive sheet (the gray arrow) produces a perfectly absorbing structure (the red dot) for the normal incidence ($\theta = 0$). Note that the reflected magnetic field depends on the incident magnetic field as

$$H_{\rm ref} = \frac{Y_{\rm in} - 1/\eta_0}{Y_{\rm in} + 1/\eta_0} H_{\rm inc}. \qquad (2)$$

When we increase losses keeping the structure at resonance, the admittance $Y_{\rm in}$ is a real number and increases from zero to $1/\eta_0$, so that eventually the perfect-absorption condition is satisfied. Obviously, the reflection coefficient remains real and negative, indicating that the reflected magnetic field is out of phase with the incident magnetic field also for lossy layers. This confirms that our structure indeed behaves as a "lossy magnetic conductor." For higher levels of losses, the sign is reversed, and in the limit of $Y_{\rm in} \to \infty$ we emulate the electric wall (perfect electric conductor).

Alternatively, and *by adopting a more realistic approach*, one can build a perfect absorber (the red dot) in the visible range by considering a lossy metallic substrate behaving as a plasmonic material at optical frequencies (the green dot) and combine it with one or multiple layers (the red arrow) which may also be lossy. This is the object of the following discussion and the results, obtained both analytically and experimentally. It is worthwhile to stress the difference between the object of the present study, which is a unilateral nonsymmetric absorber,

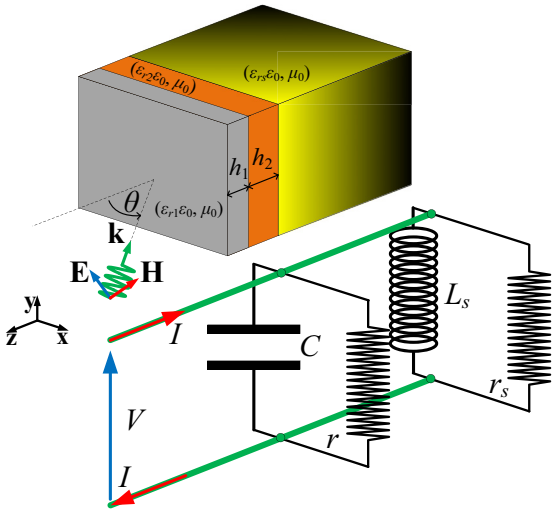

FIG. 3. (Color online) The physical configuration of the resonant absorbing structure. Two semiconducting layers of thicknesses h_1,h_2 and relative permittivities $\varepsilon_{\rm r1}$,$\varepsilon_{\rm r2}$ are installed on a metallic substrate with the permittivity $\varepsilon_{\rm rs}$ illuminated by an obliquely incident plane wave (**E**,**H**,**k**) at the angle θ. The corresponding transmission-line circuit (voltage V, current I) is also shown with a lossy capacitor (C,r) representing the role of the dielectric layers and a lossy inductor ($L_{\rm s}$,$r_{\rm s}$) representing the effect of the metallic substrate.

and the so-called coherent perfect absorber [23]. The last one is a bilaterally excited lossy structure, while the structure proposed in this paper is illuminated from one side, and the absorption takes place both in the covering dielectric layer and in the metal substrate.

B. Perfect absorber design

Let us consider one of the simplest possible absorbing configurations: the one depicted in Fig. 3. Two (magnetically inert) homogeneous dielectric layers of relative permittivities $\varepsilon_{\rm r1}$,$\varepsilon_{\rm r2}$ and thicknesses h_1,h_2 are deposited above a lossy metallic substrate characterized by complex relative permittivity $\varepsilon_{\rm rs}$. The reason for using two dielectric slabs instead of just one has to do with the experimental manufacturing issues and will become obvious in the following. Similarly to the above, we assume optically thin slabs (k_0h_1,$k_0h_2 \ll 1$), and the condition for perfect absorption is written as the *resonance* in the formulated equivalent circuit between the lossy inductor representing the currents flowing in the metal and the lossy capacitors emulating the behavior of the two thin dielectric layers:

$$Y_{\rm in}\eta_0 = \sqrt{\varepsilon_{\rm rs}} - i(\varepsilon_{\rm r1} - 1)k_0h_1 - i(\varepsilon_{\rm r2} - 1)k_0h_2 = 1. \qquad (3)$$

In this case, the two lossy parts are chosen to provide a *matched* interface with free space, in contrast to (1) where the imaginary parts of admittances are negligible. In Fig. 3, we can see also the equivalent circuit which is formulated. The dielectric layers constitute a lossy capacitive load with $C = \frac{(\mathrm{Re}[\varepsilon_{\rm r1}]-1)k_0h_1+(\mathrm{Re}[\varepsilon_{\rm r2}]-1)k_0h_2}{2\pi f\eta_0}$ and $r = \frac{\eta_0}{k_0h_1\mathrm{Im}[\varepsilon_{\rm r1}]+k_0h_2\mathrm{Im}[\varepsilon_{\rm r2}]}$, while the metallic substrate is playing the inductive role with the effective surface inductance $L_{\rm s} = \frac{\eta_0}{2\pi f\mathrm{Im}[\sqrt{\varepsilon_{\rm rs}}]}$ and $r_{\rm s} = \frac{\eta_0}{\mathrm{Re}[\sqrt{\varepsilon_{\rm rs}}]}$. The structure is fed by the voltage V (developed

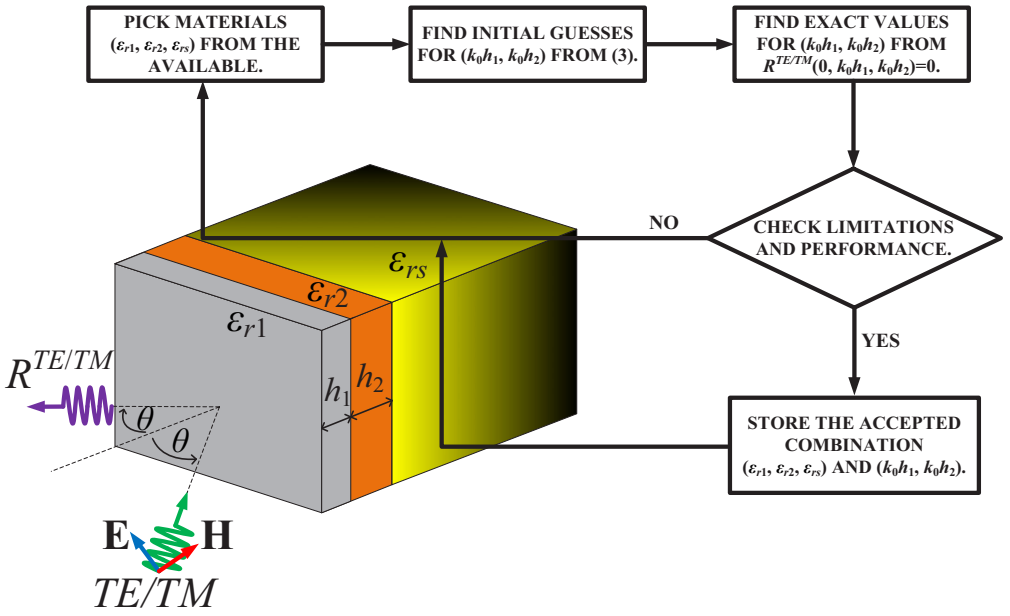

FIG. 4. (Color online) The flow chart describing how alternative material combinations leading (with the optimal thicknesses) to perfect absorbers are being derived. The thickness parameters (h_1,h_2), the material parameters (ε_{r1},ε_{r2},ε_{rs}), and the reflection coefficient $R^{TE,TM}$ as function of the incidence angle θ are again defined in the inset.

from the electric field **E**) and the current I (developed from the magnetic field **H**).

The assumption of thin slabs is sensible since we are seeking for the most compact thickness exhibiting substantial resonant absorbing performance. Furthermore, the analytical expressions for the exact reflection coefficients under oblique TE and TM excitation are well known, $R^{TE,TM}(\theta,k_0h_1,k_0h_2)$, but not rigorously presented here for brevity. Equation (3) allows us to determine for what metals and for what frequency ranges the regime of full absorption in optically thin sheets is possible. Equation (3) can be satisfied only if the real part of the refractive index of the metal substrate is smaller than unity, because for any passive materials used as dielectric covers the imaginary part of the permittivity is positive. This necessary condition is satisfied for some noble metals in the visible frequency range.

For a given set of materials (ε_{r1},ε_{r2},ε_{rs}), the complex equation (3) can give initial guesses for the optical thicknesses k_0h_1,k_0h_2 which can lead to the numerical solution of the transcendental equation $R^{TE}(0,k_0h_1,k_0h_2) = R^{TM}(0,k_0h_1,k_0h_2) = 0$. In this way, one can find the optimal combination of materials (ε_{r1},ε_{r2},ε_{rs}) and thicknesses (k_0h_1,k_0h_2) which forms a perfect absorber for $\theta = 0$ (normal incidence). From the experimental point of view, we can find several combinations of media and sizes that substantially absorb the incident illumination for $\theta = 0$ by following the flow chart of Fig. 4. From the database of the available metals and dielectrics, we fix the permittivities (ε_{r1},ε_{r2},ε_{rs}) and find the optimal sizes (k_0h_1,k_0h_2). If the layered structure with this combination of materials and thicknesses is physically realizable and acceptably optically thin, we store the configuration; otherwise we drop it and move to the next candidate. In this way, one obtains a number of different optically thin and almost perfect absorbers within the experimental limitations. The latter feature is very important since at optical frequencies where the physical sizes are *nanometer sensitive*, coherence between two consecutive layers is not always possible. For example, with the use of molecular beam epitaxy techniques, the dielectric layers can be grown *only on certain substrates* [24]. Therefore, the use of a single slab as an effective capacitor is ruled out. On the other hand, when adopting *e*-beam [25] or atomic layer deposition (ALD) [26] methods, the thickness and the quality of the sheets are *not easily controlled*.

The aforementioned iterative procedure has been applied for the available materials and we concluded that a structure comprised of a gold (effectively semi-infinite) substrate, a thin layer of germanium (Ge) with $h_2 = 6$ nm, and a thicker layer of silicon nitride (SiN_x) with $h_1 = 28$ nm behaves similarly to a perfect absorber for $f \cong 750$ THz (or $\lambda_0 \cong 400$ nm)

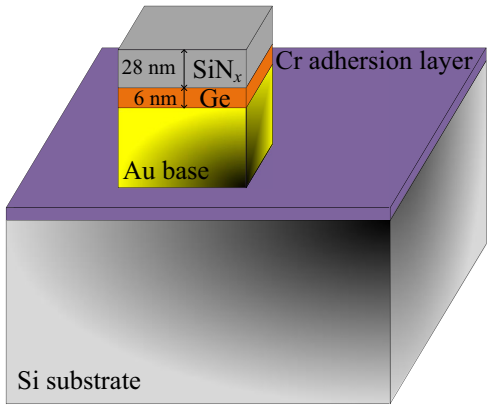

FIG. 5. (Color online) The schematic layer sequence for the grown prototype. A thin adhesion layer of Cr, 150 nm of gold, and $h_2 = 6$ nm of Ge were first grown onto a silicon substrate using the standard *e*-beam evaporation technique. Finally, the sample was transferred to a plasma-enhanced vapor phase deposition (PECVD) system with Oxford Plasmalab 80 for growth of $h_1 = 28$ nm of SiN_x.

and normal incidence ($\theta = 0$). The schematic layer sequence for the grown prototype is depicted in Fig. 5. We do not show the actual equipment setup since the measurements were done using a commercial reflectance measurement tool (Lambda-1050 instrument) and the sample exists within a closed enclosure when the measurement is run (not visible). The Ge was first grown onto a silicon substrate by standard e-beam evaporation technique in the first place. To this end, the sample was transferred to a plasma-enhanced vapor phase in order to develop the dielectric layer of SiN_x. In the following numerical results, the angle-dependent reflectance measurements were carried out using a commercial Perkin-Elmer Lambda 1050 spectrophotometer equipped with a universal reflectance accessory (URA) module. The URA module was used for specular reflectance measurements on the samples at incidence angles ranging from 10° to 60°. The angular-dependent reflectance spectra for s-polarized (TE incident wave with respect to the **z** axis) and p-polarized (TM incident wave with respect to the **z** axis) light rays were measured at wavelengths between 350 and 880 nm.

The thickness of gold is finite and equal to 150 nm. However, this feature does not affect the model of the semi-infinite metal substrate. Indeed, gold at the considered frequencies is characterized by a skin depth of about 40 nm, and over the distance 150 nm the wave transmitted into the gold layer decays by more than 99.9%. The internal reflection from the bottom surface makes the power transmitted through the gold film fully negligible.

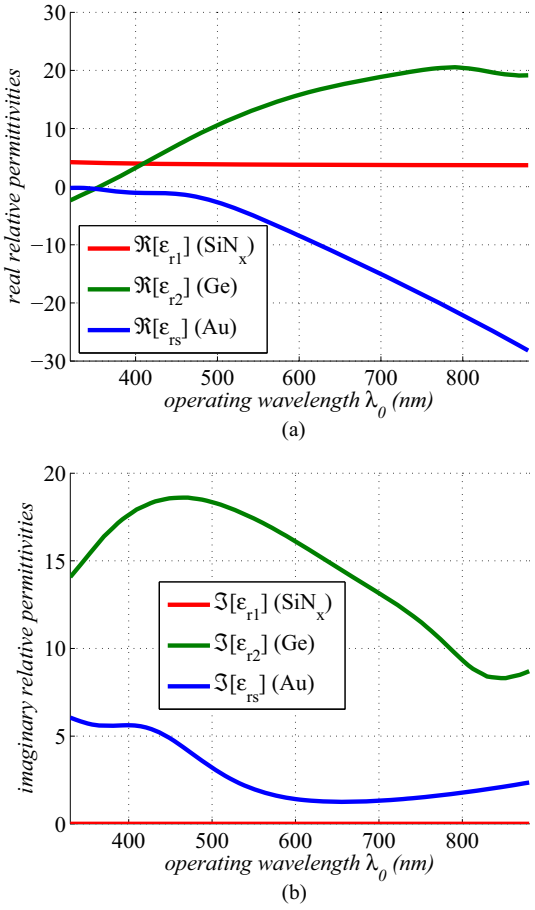

FIG. 6. (Color online) The (a) real and (b) imaginary parts of the relative permittivities of silicon nitride, ε_{r1}, germanium, ε_{r2} (as measured by our ellipsometric procedure), and gold, ε_{rs}, with respect to the operating free-space wavelength λ_0. Normal incidence: $\theta = 0$.

III. NUMERICAL AND EXPERIMENTAL RESULTS

Prior to proceeding with the representation of the absorber response, we performed ellipsometric measurements for the permittivity of a thin layer of Ge when it is sandwiched between the gold substrate and the SiN_x superstrate. As far as the permittivities of the silicon nitride and gold, they have been long established [27,28]. The variations of the relative dielectric constants of the three participating materials with respect to the operating free-space wavelength λ_0 are shown in Figs. 6(a) (real parts) and 6(b) (imaginary parts). One can clearly observe the opposite sign in the real parts of the permittivities of Au and Ge and simultaneously the different level of losses between the two materials. Note also the almost invariant behavior of SiN_x, which is lossless.

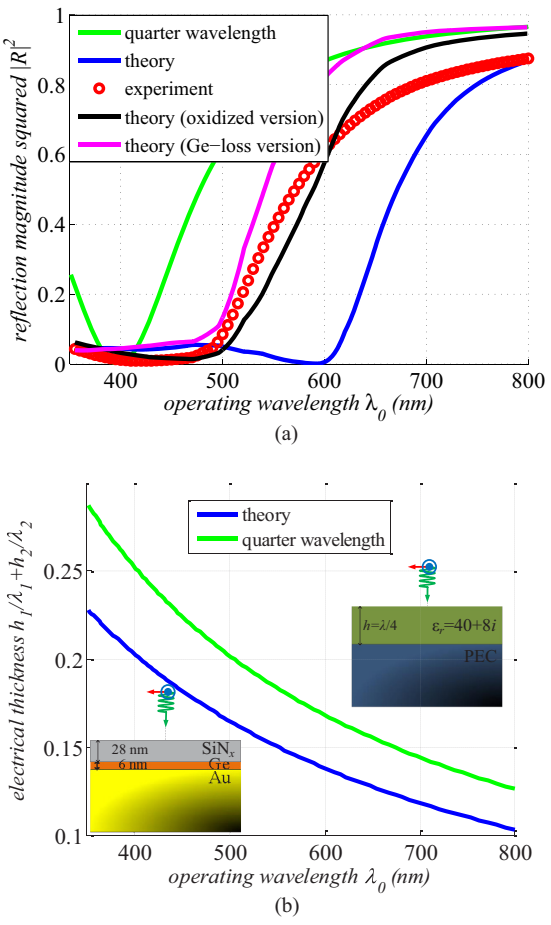

FIG. 7. (Color online) (a) The squared magnitude of the reflection coefficient $|R|^2$ for the prototype absorber (various versions of theoretical evaluations and experimental measurements) and in the case of a common quarter-wavelength (Dallenbach) absorber centralized at $\lambda_0 \cong 400$ nm with the permittivity $\varepsilon_r = 40 + i8$ and (b) the optical thickness of the two aforementioned absorbers, for varying operating free-space wavelength λ_0. Normal incidence: $\theta = 0$. The two alternative configurations are depicted in the insets of Fig. 7(b).

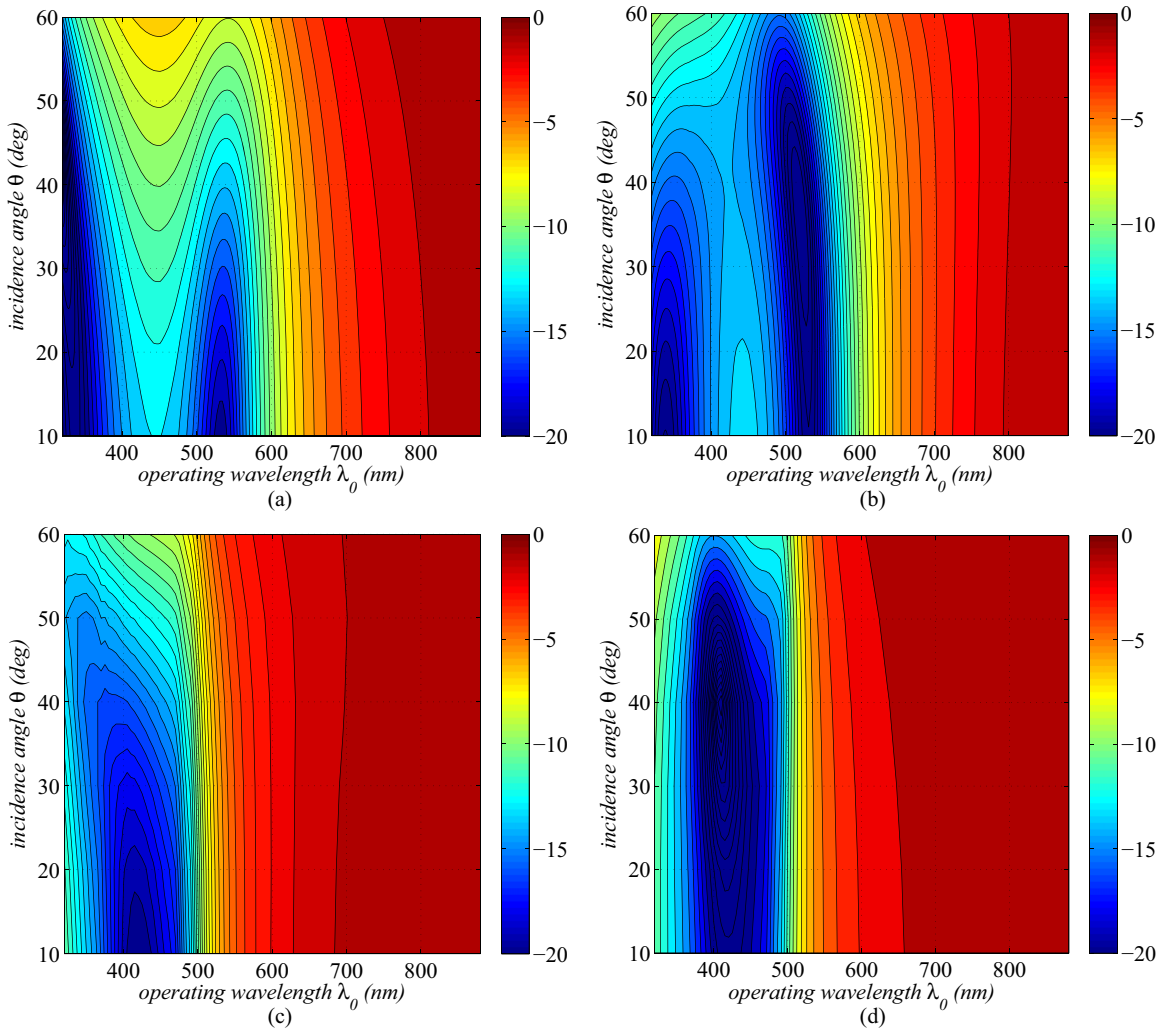

FIG. 8. (Color online) The magnitude of the squared reflection coefficient $|R^{\mathrm{TE,TM}}|^2$ (expressed in dB) in contour plots with respect to the operating free-space wavelength λ_0 and the incidence angle θ for (a) TE excitation (theory), (b) TM excitation (theory), (c) TE excitation (experiment), and (d) TM excitation (experiment).

In Fig. 7(a), we show the variation of the reflectance (squared magnitude of the reflection coefficient) $|R|^2$, under normal incidence, $\theta = 0$, with respect to the operational wavelength λ_0, for our design when analytical calculations (blue curve) and experimental measurements (red dots) are carried out. For both sets of data we remark an almost perfect absorbing effect ($|R|^2 < 0.01$) for an extensive band: 350 nm $< \lambda_0 <$ 500 nm containing entirely the violet and the blue zones and partially the green one. For larger wavelengths, the performance of the device deteriorates and strongly reflects the incident illumination. To evaluate the size of the functional frequency band of the device, we consider a common quarter-wavelength absorber [21], namely, a grounded dielectric slab with a large relative permittivity $\varepsilon_{\mathrm{r}} = 40 + i8$ and thickness h equal to a quarter of the effective wavelength at $f \cong 750$ THz, namely, $h = \frac{\lambda}{4} = \frac{c}{4f\sqrt{\mathrm{Re}[\varepsilon_{\mathrm{r}}]}}$. In the same graph, we show its response with green color and notice that we obtain zero reflection for the central wavelength $\lambda_0 \cong 450$ nm, but the operational band is much narrower than in our prototype. Therefore, we directly conclude that the proposed prototype is over three times more wideband than conventional structures. The difference between the theory and the actual data can be attributed to the fact that the Ge layer, during the PECVD of SiN_x, most likely oxidizes to a certain depth (5–6 nm) and loses the indicated properties, namely, its refractive index gets smaller (equal to that of GeO_x) and the losses become negligibly small in this oxidized layer. For this reason, we show (black curve) also the response of the oxidized Ge layer (6 nm GeO_x and only 1 nm Ge) and we notice that the coincidence of the corresponding curve with the measured data (red dots) is better. Furthermore, we represent (purple curve) the response of the system in the total absence of germanium (28 nm of SiN_x on a gold base) and we notice that an imperfect broadband absorber is formulated without adding losses to those of gold (the resistance remains much smaller than η_0). This confirms that the boost of absorption by ten times (the reflectionof 40% becomes 4%) is indeed due to neutralization of reactance (the kinetic inductance of gold is compensated by the effective capacitance of the SiN_x film).

In Fig. 7(a), we represent the optical thickness $\frac{h_1}{\lambda_1} + \frac{h_2}{\lambda_2}$ of our combined film by evaluating the effective wavelengths λ_1, λ_2 inside each material (SiN_x, Ge, respectively), as functions

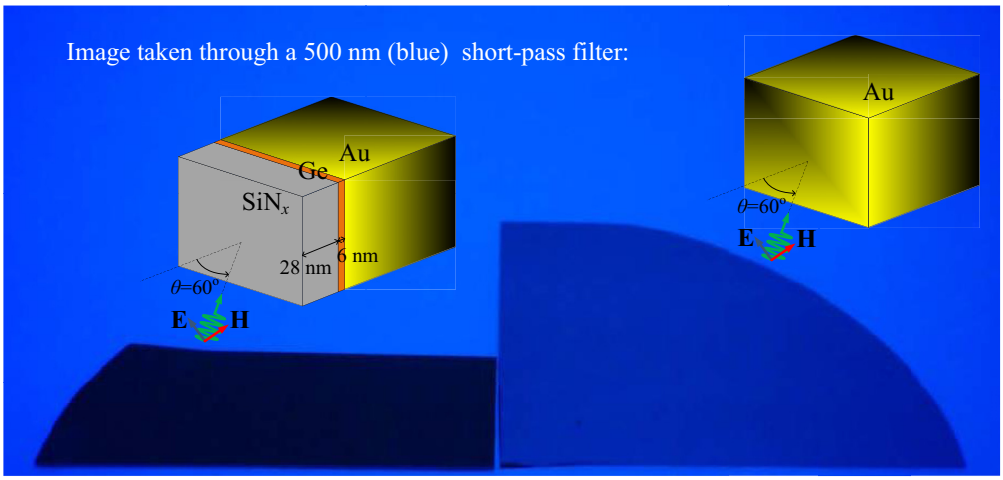

FIG. 9. (Color online) A demonstration of the absorbing efficiency of the prototype. Blue light ($\lambda_0 \cong 500$ nm) illuminates at the angle $\theta = 60^\circ$ both our prototype (left) and a gold reference sheet (right). Our device even at the extreme limits of its operation (very large wavelength and very oblique incidence) appears working nicely. The two alternative configurations are depicted in the insets.

of the free-space operational wavelength λ_0. We compare the results with the corresponding ones of the aforementioned quarter-wavelength absorber. We see that at each frequency our device is optically thinner than common absorbers. The difference would be much larger in favor of our prototype if we considered only the optical thickness of the Ge slab, $\frac{h_2}{\lambda_2}$, which does the main absorbing job (the SiN_x layer is employed mainly to ease the manufacturing).

To summarize the above results, we have fabricated an absorber which is (i) *very efficient* ($|R|^2 < 0.01$), (ii) *extremely broadband* (350 nm $< \lambda_0 <$ 500 nm), (iii) *optically thin* ($\frac{h_1}{\lambda_1} + \frac{h_2}{\lambda_2} < 0.2$), and, above all, (iv) *very simple* as a structure without nanoparticles, separate components, or other complicated equipment. Let us next test its endurance with respect to the incidence angle θ, since, in the above, we have assumed normally incident illumination ($\theta = 0$). In Fig. 8, we show the reflectance $|R|^2$ (expressed in dB) in contour plots with respect to the operating free-space wavelength λ_0 and the incidence angle θ for the TE excitation [the incident electric field $\mathbf{E}_{\text{inc}}$ normal to the **z** axis, Fig. 8(a)] and the TM excitation [the incident magnetic field $\mathbf{H}_{\text{inc}}$ normal to the **z** axis, Fig. 8(b)]. We can also compare the analytical calculations of Figs. 8(a) and 8(b) with the corresponding experimental data of Figs. 8(c) and 8(d). It is directly noticed that for both excitations our prototype exhibits substantial robustness with respect to the incident angle θ, a feature that means that the proposed device could work as a quasiperfect absorber for almost arbitrary incidence illumination. Especially in the actual experimental test, we note that the prototype can absorb at least 92% of power from the incoming rays existing within the wide cone $0 < \theta < 60^\circ$ and at the same time signals with the main harmonic content within the wide interval $300 < \lambda_0 < 500$ nm ($600 < f < 1000$ THz).

To demonstrate the efficiency of our experimental structure, we selected a quite challenging combination of frequency and incidence angle. In particular, we considered low-frequency light blue radiation with $\lambda_0 \cong 500$ nm, namely, at the upper limit of the operational wavelength band, propagating along the direction $\theta = 60^\circ$, that is, at the upper limit of the absorbing cone. The response of our structure, in comparison with a gold reference plane, is shown in Fig. 9. It is apparent that, even under this illumination, which is very far from the central functional point of our device, the prototype *absorbs the vast portion* of the incoming electromagnetic power as

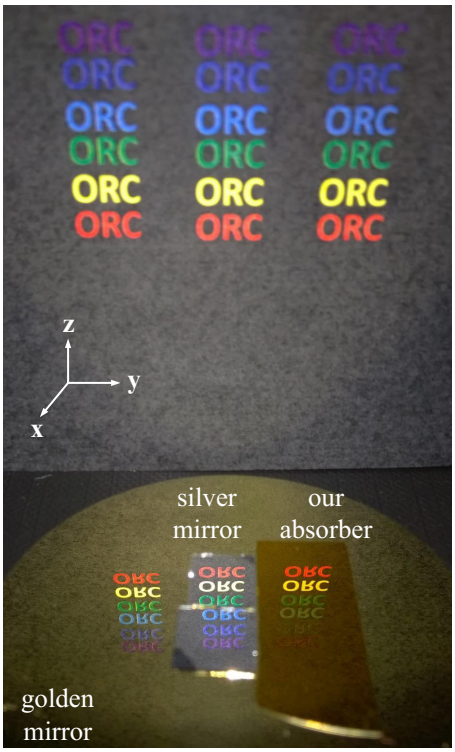

FIG. 10. (Color online) A demonstration of the absorbing efficiency of the present prototype with respect to various frequencies. The reflection of a colored text on a black surface (a piece of paper in this case) has been captured (i) when only the gold substrate is present, (ii) when a silver mirror is posed on the top, and (iii) when using our prototype sample. It is clear that our absorber is very efficient for blue, violet, and ultraviolet radiation but reflects strongly at smaller frequencies (green, yellow, red).

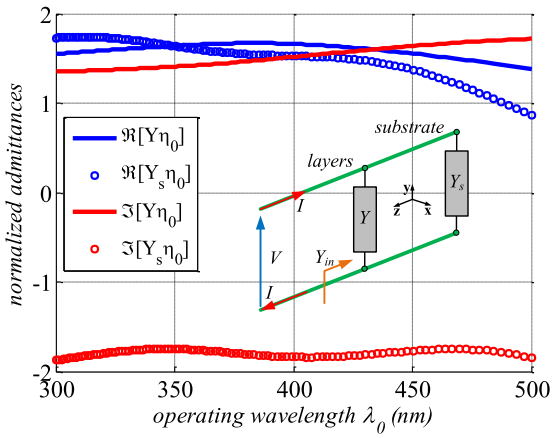

FIG. 11. (Color online) The (real and imaginary) normalized admittances of the capacitive layers (SiN_x, Ge) and inductive substrate (Au) as functions of the operating free-space wavelength λ_0. Normal incidence: $\theta = 0$. The definitions of the input admittance Y_{in}, the admittance of the semiconducting layers Y, and the admittance of the metallic bulk Y_s are given in the inset of the transmission-line circuit (voltage V, current I).

indicated by its black color. In contrast the gold reference patch is (a bit lighter) blue which means that most of the incident illumination is reflected back. To test the absorption performance of our structure, we took a photograph (Fig. 10) of it, when illuminated by optical waves constituting a colored text. The sample is posed on the gold base (gold mirror) in order to compare the two responses, while an alternative perfect reflector (silver mirror) is also used for understanding the absorbing efficiency of the structure. By inspection of Fig. 10, it is obvious that the sample *absorbs almost completely the blue and violet radiation* ($350 < \lambda_0 < 550$ nm) and almost totally reflects the incident illumination (as mirrors do) with larger wavelengths (green, yellow, red, namely, $550 < \lambda_0 < 800$ nm).

Returning to our initial consideration which led to the semianalytical formula (3), it is instructive to consider the equivalent circuit of the structure for normal incidence ($\theta = 0$) in an attempt to understand the mechanism managing such a high and wideband (with respect to both f and θ) absorbing efficiency with so simple a structure. In Fig. 11, we represent the real and the imaginary parts of the normalized admittance which approximately, according to (3), describe the circuit equivalents of the dielectric layers $Y\eta_0 = -[ik_0h_1(\varepsilon_{r1} - 1) + ik_0h_2(\varepsilon_{r2} - 1)]$ and the gold substrate $Y_s\eta_0 = \sqrt{\varepsilon_{rs}}$, as functions of the free-space wavelength λ_0. We can notice that over the entire absorbing band $300 < \lambda_0 < 500$ nm, the imaginary parts of the two admittances are almost *opposite each other*, a feature which demonstrates and explains the wideband resonant nature of the absorber.

IV. CONCLUSIONS

Designing and constructing magnetic conductors and absorbers in the optical frequency range is a challenging task due to the absence of magnetic charges and finite conductivity of the metals used to create artificial magnetics. In this work, we have introduced the concept of an internal-inductance high-impedance surface and magnetic conductor for the visible range, exploring the negative permittivity of metals in combination with positive permittivity of dielectrics. In particular, we have shown how a parallel-circuit resonance of a dielectric layer on a metal substrate can be exploited to create a nearly perfect absorber. We have designed and studied a very simply realizable structure which possesses the properties of a lossy magnetic wall in a wide frequency band for both polarizations and many incidence angles. To facilitate understanding and design, we have developed a very simple resonant circuit model formulated between the inductive response of the currents flowing in a metallic base and the capacitive influence of a thin lossy dielectric layer. The optimal thicknesses of the layers are chosen by numerical optimization based on initial estimations provided by our models. Numerous combinations of available materials have been tested, and one of the possible designs (a gold substrate capped by a layer of germanium grown on a silicon oxide base) has been fabricated and measured. The substantial absorbing efficiency predicted with the use of the analytical model has been verified experimentally. The performance of the device remains high within the entire violet and blue frequency bands and is practically independent of the polarization of the electromagnetic illumination and the angle of incidence.

Practical applications of this optical absorber configuration and the accompanying physical insight and explanations and interpretations may shed light upon the design, modeling, and construction of ultrathin photodetectors and solar cells with better effectiveness. The present approach also paves the way for understanding and new designs when considering various electromagnetic processing devices in the optical frequencies. In particular, similar equivalent-circuit models can be developed for a variety of optical structures (lenses, cloaks, controllers) in order to find ways for semianalytical optimizations. Finally, the inverse search for the most suitable materials exhibiting certain properties and satisfying cost or fabrication constraints, which has been used in the presented study, can be easily utilized for alternative purposes.

ACKNOWLEDGMENTS

The authors acknowledge Dr. Pertti Pääkkönen from University of Eastern Finland for determining the parameters of the germanium films by ellipsometry.

[1] A. Erentok, P. L. Luljak, and R. W. Ziolkowski, Characterization of a volumetric metamaterial realization of an artificial magnetic conductor for antenna applications, IEEE Trans. Antennas Propag. **53**, 160 (2005).

[2] O. Luukkonen, C. R. Simovski, and S. A. Tretyakov, Grounded uniaxial material slabs as magnetic conductors, Prog. Electromagn. Res. B **15**, 267 (2009).

[3] D. Sievenpiper, L. Zhang, R. F. J. Broas, N. G. Alexopoulos, and E. Yablonovitch, High-impedance electromagnetic surfaces with a forbidden frequency band, IEEE Trans. Microwave Theory Tech. **47**, 2059 (1999).

[4] F.-R. Yang, K.-P. Ma, Y. Qian, and T. Itoh, A. novel TEM waveguide using uniplanar compact photonic-bandgap (UC-PBG) structure, IEEE Trans. Microwave Theory Tech. **47**, 2092 (1999).

[5] O. Luukkonen, C. Simovski, G. Granet, G. Goussetis, D. Lioubtchenko, A. V. Räisänen, and S. A. Tretyakov, Simple and accurate analytical model of planar grids and high-impedance surfaces comprising metal strips or patches, IEEE Trans. Antennas Propag. **56**, 1624 (2008); Corrections to "Simple and Accurate Analytical Model of Planar Grids and High-Impedance Surfaces Comprising Metal Strips or Patches", IEEE Trans Antennas Propag. **58**, 2162 (2010).

[6] A. P. Feresidis, G. Goussetis, S. Wang, and J. C. Vardaxoglou, Artificial magnetic conductor surfaces and their application to low-profile high-gain planar antennas, IEEE Trans. Antennas Propag. **53**, 209 (2005).

[7] M. A. Hiranandani, A. B. Yakovlev and A. A. Kishk, Artificial magnetic conductors realised by frequency-selective surfaces on a grounded dielectric slab for antenna applications, IEE Proc.—Microwaves, Antennas, Propag. **153**, 487 (2006).

[8] S. A. Tretyakov and S. I. Maslovski, Thin absorbing structure for all incidence angles based on the use of a high-impedance surface, Microwave Opt. Technol. Lett. **40**, 209 (2004).

[9] A. S. Schwanecke, V. A. Fedotov, V. V. Khardikov, S. L. Prosvirnin, Y. Chen and N. I. Zheludev, Optical magnetic mirrors, J. Opt. A: Pure Appl. Opt. **9**, L1 (2007).

[10] H. Rostami, Y. Abdi, and E. Arzi, Fabrication of optical magnetic mirrors using bent and mushroom-like carbon nanotubes, Carbon **48**, 3659 (2010).

[11] S. Liu, M. B. Sinclair, T. S. Mahony, Y. C. Jun, S. Campione, J. Ginn, D. A. Bender, J. R. Wendt, J. F. Ihlefeld, P. G. Clem, J. B. Wright, and I. Brener, Optical magnetic mirrors without metals, Optica **1**, 250 (2014).

[12] N. Engheta, Thin absorbing screens using metamaterial surfaces, in *Proceedings of the IEEE Antennas and Propagation Society International Symposium, San Antonio, TX* (IEEE, New York, 2002), Vol. 2, p. 392.

[13] G. Li, X. Chen, O. Li, C. Shao, Y. Jiang, L. Huang, B. Ni, W. Hu, and W. Lu, A. novel plasmonic resonance sensor based on an infrared perfect absorber, J. Phys. D **45**, 205102 (2012).

[14] N. Liu, H. Guo, L. Fu, S. Kaiser, H. Schweizer, and H. Giessen, Plasmon hybridization in stacked cut-wire metamaterials, Adv. Mater. **19**, 3628 (2007).

[15] J. Dai, F. Ye, Y. Chen, M. Muhammed, M. Qiu, and M. Yan, Light absorber based on nano-spheres on a substrate reflector, Opt. Express **21**, 6697 (2013).

[16] N. Liu, M. Mesch, T. Weiss, M. Hentschel, and H. Giessen, Infrared perfect absorber and its application as plasmonic sensor, Nano Lett. **10**, 2342 (2010).

[17] X. Liu, T. Starr, A. F. Starr, and W. J. Padilla, Infrared spatial and frequency selective metamaterial with near unity absorbance, Phys. Rev. Lett. **104**, 207403 (2010).

[18] J. W. Park, P. V. Tuong, J. Y. Rhee, K. W. Kim, W. H. Jang, E. H. Choi, L. Y. Chen, and Y. P. Lee, Multiband metamaterial absorber based on the arrangement of donut-type resonators, Opt. Express **21**, 9691 (2013).

[19] M. A. Kats, R. Blanchard, P. Genevet, and F. Capasso, Nanometre optical coatings based on strong interference effects in highly absorbing media, Nat. Mater. **12**, 20 (2012).

[20] J. Park, J.-H. Kang, A. P. Vasudev, D. T. Schoen, H. Kim, E. Hasman, and M. L. Brongersma, Omnidirectional near-unity absorption in an ultrathin planar semiconductor layer on a metal substrate, ACS Photonics **1**, 812 (2014).

[21] W. Dallenbach and W. Kleinsteuber, Reflection and absorption of decimeter-waves by plane dielectric layers, Hochfrequenztech. Elektroakust. **51**, 152 (1938).

[22] C. A. Valagiannopoulos and A. Sihvola, Low-pass features of optical nano-filters constituted by simple layered structures, Microwave Opt. Technol. Lett. **55**, 2099 (2013).

[23] Y. D. Chong, L. Ge, H. Cao, and A. D. Stone, Coherent perfect absorbers: time-reversed lasers, Phys. Rev. Lett. **105**, 053901 (2010).

[24] L. N. Pfeiffer, K. W. West, R. L. Willett, H. Akiyama, and L. P. Rokhinson, Nanostructures in GaAs fabricated by molecular beam epitaxy, Bell Labs Tech. J. **10**, 151 (2005).

[25] V. Sivakova, F. Heyrothc, F. Falkb, G. Andra, and S. Christiansena, Silicon nanowire growth by electron beam evaporation: kinetic and energetic contributions to the growth morphology, J. Cryst. Growth **300**, 288 (2007).

[26] C. M. Wang, D. L. Kong, Q. Chen, and J. M. Xue, Surface engineering of synthetic nanopores by atomic layer deposition and their applications, Front. Mater. Sci. **7**, 335 (2013).

[27] A. D. Rakic, A. B. Djurisic, J. M. Elazar, and M. L. Majewski, Optical properties of metallic films for vertical-cavity optoelectronic devices, Appl. Opt. **37**, 5271 (1998).

[28] D. F. Edwards and E. Ochoa, Infrared refractive indexes of silicon, Appl. Opt. **19**, 4130 (1980).